Neurobiology of Disease 127 (2019) 591–604

Contents lists available at ScienceDirect

Neurobiology of Disease

journal homepage: www.elsevier.com/locate/ynbdi

A hydrogel engineered to deliver minocycline locally to the injured cervical spinal cord protects respiratory neural circuitry and preserves diaphragm function

Biswarup Ghosh[a,1], Jia Nong[b,1], Zhicheng Wang[b], Mark W. Urban[a], Nicolette M. Heinsinger[a], Victoria A. Trovillion[a], Megan C. Wright[c], Angelo C. Lepore[a,*], Yinghui Zhong[b,**]

[a] Department of Neuroscience, Vickie and Jack Farber Institute for Neuroscience, Sidney Kimmel Medical College at Thomas Jefferson University, 233 S. 10th St., Bluemle Life Sciences Building - Room 245, Philadelphia, PA 19107, United States of America

[b] School of Biomedical Engineering, Science and Health Systems, Drexel University, 3141 Chestnut Street, Bossone 7-716, Philadelphia, PA 19104, United States of America

[c] Department of Biology, Arcadia University, 450 S Easton Rd, 220 Boyer Hall, Glenside, PA 19038, United States of America

ARTICLE INFO

Keywords:
Cervical
Spinal cord injury
Contusion
Phrenic motor neuron
Diaphragm
Respiratory
Minocycline
Biomaterials
Hydrogel
Drug delivery

ABSTRACT

We tested a biomaterial-based approach to preserve the critical phrenic motor circuitry that controls diaphragm function by locally delivering minocycline hydrochloride (MH) following cervical spinal cord injury (SCI). MH is a clinically-available antibiotic and anti-inflammatory drug that targets a broad range of secondary injury mechanisms via its anti-inflammatory, anti-oxidant and anti-apoptotic properties. However, MH is only neuroprotective at high concentrations that cannot be achieved by systemic administration, which limits its clinical efficacy. We have developed a hydrogel-based MH delivery system that can be injected into the intrathecal space for local delivery of high concentrations of MH, without damaging spinal cord tissue. Implantation of MH hydrogel after unilateral level-C4/5 contusion SCI robustly preserved diaphragm function, as assessed by in vivo recordings of compound muscle action potential (CMAP) and electromyography (EMG) amplitudes. MH hydrogel also decreased lesion size and degeneration of cervical motor neuron somata, demonstrating its central neuroprotective effects within the injured cervical spinal cord. Furthermore, MH hydrogel significantly preserved diaphragm innervation by the axons of phrenic motor neurons (PhMNs), as assessed by both detailed neuromuscular junction (NMJ) morphological analysis and retrograde PhMN labeling from the diaphragm using cholera toxin B (CTB). In conclusion, our findings demonstrate that local MH hydrogel delivery to the injured cervical spinal cord is effective in preserving respiratory function after SCI by protecting the important neural circuitry that controls diaphragm activation.

Abbreviations: 5-HT, 5-hydroxytryptamine (serotonin); ALS, amyotrophic lateral sclerosis; AP-1, activator protein 1; Arg1, arginase 1; ATF2, activating transcription factor 2; BDNF, brain-derived neurotrophic factor; C3, 4, 5, cervical spinal cord level 3 (4, 5, etc.); CMAP, compound muscle action potential; COX-2, cyclooxygenase-2; CSF, cerebrospinal fluid; CSPGs, chondroitin sulfate proteoglycans; CTB, cholera toxin B subunit; DS, dextran sulfate; EMG, electromyography; HBSS, Hank's Balanced Salt Solution; IL-1β, interleukin-1β; IL-6, interleukin-6; iNOS, inducible nitric oxide synthase; LITAF, lipopolysaccharide-induced tumor necrosis factor-alpha factor; LOX-1, low density lipoprotein receptor-1; MH, minocycline hydrochloride; MMP, matrix metalloproteinase; mPTP, mitochondrial permeability transition pore; NADPH, nicotinamide adenine dinucleotide phosphate; NF-κB, nuclear factor kappaB; NMDA, *N*-methyl-D-aspartate; NMJ, neuromuscular junction; NO, nitric oxide; NT-3, neurotrophin-3; Nur77, nerve growth factor IB; p38 MAPK, p38 mitogen-activated protein kinases; PARP-1, poly(ADP-ribose) polymerase-1; PhMN, phrenic motor neuron; PI3K, phosphoinositide 3-kinase; ROS, reactive oxygen species; rVRG, rostral ventral respiratory group; SCI, spinal cord injury; SV2, synaptic vesicle protein 2; TNFα, tumor necrosis factor α

* Correspondence to: A.C. Lepore, Department of Neuroscience, Vickie and Jack Farber Institute for Neuroscience, Sidney Kimmel Medical College at Thomas Jefferson University, 233 S. 10th St., Bluemle Life Sciences Building - Room 245, Philadelphia, PA 19107, United States of America

** Correspondence to: Y. Zhong, School of Biomedical Engineering, Science and Health Systems, Drexel University, 3141 Chestnut Street, Bossone 7-718, Philadelphia, PA 19104, United States of America

E-mail addresses: angelo.lepore@jefferson.edu (A.C. Lepore), yz348@drexel.edu (Y. Zhong).

[1] Authors contributed equally to this work.

https://doi.org/10.1016/j.nbd.2019.04.014
Received 27 November 2018; Received in revised form 6 April 2019; Accepted 23 April 2019
Available online 25 April 2019
0969-9961/

1. Introduction

A major portion of human spinal cord injury (SCI) cases is contusive in nature and affects mid-cervical levels (Nobunaga et al., 1999; Hulsebosch, 2002; Lane et al., 2008), the location of the important pool of phrenic motor neurons (PhMNs) that innervate the diaphragm, the primary muscle of inspiration (Nicaise et al., 2013). Ventilatory insufficiency and associated complications are primary causes of both morbidity and mortality after SCI (Shanmuganathan et al., 2008). Initial contusive cervical spinal cord trauma is followed by a period of pronounced secondary degeneration of PhMNs and consequent denervation at the diaphragm neuromuscular junction (NMJ), as well as damage to the descending bulbospinal axons that activate PhMNs, resulting in debilitating and often chronic respiratory compromise. A valuable opportunity therefore exists following cervical SCI for preventing PhMN loss, axon damage and synaptic disconnection that occur during secondary degeneration and consequently preserving respiratory function.

A number of mechanisms are involved in the secondary injury cascades following SCI, including inflammation, reactive oxygen species (ROS) and nitric oxide (NO), glutamate excitotoxicity, calcium influx, mitochondrial dysfunction, ischemia, and hemorrhage (Oyinbo, 2011; Shultz and Zhong, 2017; Teng et al., 2004). However, most current strategies only target one or a few elements in the injury cascades, and have been largely unsuccessful in clinical trials. MH is a clinically-available anti-inflammatory drug that also has potent neuroprotective activities (Garrido-Mesa et al., 2013; Kim and Suh, 2009; Stirling et al., 2005). It targets the aforementioned injury mechanisms via its anti-inflammatory, anti-oxidant, and anti-apoptotic properties (Teng et al., 2004; Amin et al., 1996; Garcia-Martinez et al., 2010; Kraus et al., 2005; Lee et al., 2003; Pi et al., 2004; Stirling et al., 2004; Takeda et al., 2011; Wasserman and Schlichter, 2007; Xue et al., 2010; Shultz and Zhong, 2017).

In a recent systematic review of pre-clinical data, MH was considered the highest scoring neuroprotective therapy for SCI (Kwon et al., 2011). However, a phase II clinical trial showed that the highest tolerable human dose only resulted in modest functional recovery, whereas low-dose was ineffective (Casha et al., 2012). This result is not surprising, as MH is only fully neuroprotective at high concentrations of 35–75 μg/mL (1.5–50 μg/mL for oxidative stress (Kraus et al., 2005), 5–50 μg/mL for glutamate toxicity (Wang et al., 2003), 35–75 μg/mL for mitochondria and calcium flux (Garcia-Martinez et al., 2010), and 10–40 μg/mL for hemorrhage-induced toxicity (Xue et al., 2010), in a dose-dependent manner), whereas the highest tolerable human doses used in the clinical trial only produced 2.3 μg/mL MH in the cerebrospinal fluid (CSF) at steady state (Casha et al., 2012). Therefore, the inability to translate high doses used in experimental animals to tolerable doses in patients limits its clinical efficacy.

Toward this challenge, we have developed novel dextran sulfate (DS)-MH particles self-assembled by metal ion-mediated interactions (Zhang et al., 2015). The particles can be embedded into agarose hydrogel that can be injected into the intrathecal space between the dura/arachnoid and spinal cord at the injury site for local delivery of high MH concentrations; clinically, this could possibly be delivered, for example, when a spinal surgery is performed to decompress and stabilize the spine (Wang et al., 2017). This route of drug delivery is preferred over epidural, intraparenchymal or systemic injection because it bypasses the dura as a diffusion barrier without damaging the spinal cord tissue or eliciting systemic toxicity (Shoichet et al., 2007; Wang et al., 2017). Moreover, all the materials used in the drug delivery system are biocompatible natural polysaccharides that have been shown to be safe for human use (Komai et al., 2005; Neimert-Andersson et al., 2014; Scarano et al., 2009; Nagoshi and Fehlings, 2015). We have developed a formulation capable of locally delivering high doses of MH for at least 3 days in vivo (35.7 to 24.7 μg/mL from day 1 to 3 in the local spinal cord tissue), followed by low dose for at least 18 days (Wang et al., 2017). To determine MH levels in spinal cord tissue, we measured MH concentration in the local spinal cord tissue at the lesion site using high performance liquid chromatography (HPLC). We previously showed that this formulation robustly reduced secondary injury and improved locomotor functions (i.e. forelimb locomotor function and grid walk) after cervical contusion SCI (Wang et al., 2017). In the present study, we investigated the efficacy of implantation of MH hydrogel after unilateral level-C4/5 contusion SCI in preserving diaphragm function, immunomodulation, and protecting and repairing the important respiratory neural circuitry.

2. Materials and methods

2.1. Animals

Female Sprague-Dawley rats (250–300 g; Taconic Farm, Rockville, MD) were housed in a facility that controlled for humidity, temperature, and light, and were given access to water and food ad libitum. All experimental procedures were performed in compliance with the ARRIVE guidelines and the NIH guide for the care and use of laboratory animals. Animal use protocols were approved by the Thomas Jefferson University IACUC and Drexel University IACUC. Rats were randomly assigned across laminectomy-only, contusion SCI, blank hydrogel and MH hydrogel groups in all experiments.

2.2. Unilateral cervical contusion

We previously established a well-characterized and clinically-relevant model of unilateral mid-cervical contusion SCI in the rat (Nicaise et al., 2013; Nicaise et al., 2012a). Our injury model produces robust loss of PhMNs, diaphragm denervation, and altered diaphragm activity. Rats received an intraperitoneal injection of a cocktail of ketamine (100 mg/kg), xylazine (5 mg/kg) and acepromazine (2 mg/kg); orbital and toe pinch reflexes were monitored to ensure anesthesia. Cervical dorsal skin and muscles were incised, and a hemi-laminectomy was performed on the right side of the spinal cord to expose C4/5 spinal cord. A unilateral contusion was then administered with the Infinite Horizon spinal impactor (Precision Systems and Instrumentation, Lexington, KY) using a 1.5 mm tip at a force of 395 kDynes.

2.3. Minocycline hydrogel fabrication and implantation

MH hydrogel was fabricated and implanted, as we previously reported (Wang et al., 2017). Briefly, DS was dissolved in 2× Hank's Balanced Salt Solution (HBSS). Agarose was then dissolved in DS Solution (HBSS). Chitosan was prepared in 0.1 M acetic acid and mixed with MH solution (dissolved in water). Equal amounts of agarose-DS and MH-chitosan solutions were well mixed to form particles uniformly in agarose. NaOH was added to neutralize the acid and then the mixture solution was allowed to gel at 4 °C for 30 min. MH concentration in the hydrogel was 3 mg/mL. We injected 30 μL MH hydrogel or blank hydrogel control sub-durally immediately following unilateral C4/5 contusion. Another 100 μL MH hydrogel or blank hydrogel control was applied epidurally to increase MH concentration in the spinal cord tissue.

2.4. Measurement of diaphragm CMAPs

Isoflurane (2.0–2.5% diluted in oxygen; Piramal Healthcare, Bethlehem, PA) was used to anesthetize the rats. Positive and negative stimulating needle electrodes were inserted at the neck close to the phrenic nerve either ipsilateral or contralateral to the injury and spaced 0.5 cm apart (Lepore et al., 2008; Lepore et al., 2010). A ground needle electrode was subcutaneously placed into the tail, and a reference electrode was inserted subcutaneously into the right abdominal region. A recording electrode with a surface strip was placed along the costal

margin of the diaphragm. The phrenic nerve was then stimulated (0.5 ms duration; 6 mV amplitude), and 10–20 recordings were obtained with 5 s intervals between stimulations. CMAP amplitude was measured baseline to peak. An ADI Powerlab 8/30 stimulator and BioAMP amplifier (ADInstruments, Colorado Springs, CO) were used for recordings, and Scope 3.5.6 (ADInstruments) was used to analyze data. CMAPs were measured for each animal weekly for three weeks following SCI.

2.5. EMG recordings

Isoflurane (2.0–2.5% in oxygen) was used to anesthetize the animals. The hemi-diaphragm was exposed via laparotomy either ipsilateral or contralateral to the injury. Bipolar electrodes were inserted 3 mm apart into the dorsal, medial or ventral sub-regions of the hemi-diaphragm. For each animal, activity was recorded and averaged over two minutes in order to quantify peak amplitude, burst duration, and frequency (Li et al., 2015a; Li et al., 2015b; Li et al., 2014). The EMG signal was amplified and filtered through a band-pass filter (50–3000 Hz) using LabChart 7 software (ADInstruments, Colorado Springs, CO). All EMG recordings were terminal procedures.

2.6. Retrograde labeling of PhMNs

Cholera toxin subunit B (CTB) conjugated to Alexa647 (Life Technologies, Eugene, OR) was delivered into the intrapleural space of the hemi-diaphragm ipsilateral to the contusion. CTB can then retrogradely label PhMN somata and dendrites in the ventral horn of cervical spinal cord in order to visualize the PhMN pool (Li et al., 2014; Nicaise et al., 2012a). Rats were anesthetized, and the hemi-diaphragm was exposed via laparotomy. 5 μL of 0.2% CTB solution in distilled water were injected trans-diaphragmatically into each of the dorsal, medial and ventral sub-regions of the ipsilateral hemi-diaphragm (total 15 μL per hemi-diaphragm) using a 20 μL Hamilton syringe. Abdominal muscles and skin were then sutured separately.

2.7. Diaphragm and spinal cord dissection

Animals were euthanized with ketamine (300 mg/kg), xylazine (15 mg/kg) and acepromazine (6 mg/kg) 5 weeks following SCI. The hemi-diaphragm was exposed laterally along the rib cage and then excised using spring scissors (Fine Science Tools, Foster City, CA), stretched flat, pinned down to Sylgard medium (Fisher Scientific, Pittsburgh, PA), and washed with PBS. Diaphragm was then fixed in 4% paraformaldehyde (Electron Microscopy Sciences) for 20 min, followed by a wash in PBS. Superficial fascia were then carefully removed from the surface of the diaphragm, and diaphragm muscles were processed for NMJ immunohistochemistry. After hemi-diaphragm was removed, animals were perfused with 0.9% saline solution, followed by 4% paraformaldehyde. Spinal cord and brain were dissected and post-fixed in 4% paraformaldehyde overnight at 4 °C. The tissue was then washed with 0.1 M phosphate buffer solution for 24 h and cryoprotected with a 30% sucrose solution for 3 days. The cervical spinal cord was embedded in tissue freezing medium, flash frozen, and sectioned in transverse or sagittal orientations at 20 μm thickness.

2.8. Assessment of lesion volume and ventral horn motor neurons

Transverse spinal cord sections 160 μm apart from cervical regions C3–5 were stained for Nissl bodies and myelin using cresyl violet and euriochrome cyanine, respectively. Images were acquired with a Zeiss Imager M2 upright microscope. The lesion area per section was measured using ImageJ software, and these values were used to quantify total lesion volume (Wang et al., 2017). Lesion was defined as areas including both lost tissue (cystic cavity formation) and surrounding damaged tissue in which the normal anatomical structure of the spinal cord was lost. The number of motor neuron cell bodies was quantified manually in a blinded manner. Motor neurons with a clearly identifiable nucleus and a cell soma > 200 μm^2 were counted (Wang et al., 2017). CTB-labeled PhMNs in the C3–5 ventral horn were also counted in 100 μm spaced transverse sections in a blinded manner (Li et al., 2014; Nicaise et al., 2012a).

2.9. Neuromuscular junction (NMJ) analysis

Fresh hemi-diaphragm muscle was dissected as described above and connective tissue was removed for optimum antibody penetration. Incubation with primary antibodies SMI-312R (Covance, Princeton, NJ) and SV2-s (DSHB, Iowa City, IA) followed by the FITC anti-mouse IgG secondary (Jackson ImmunoResearch Laboratories, West Grove, PA) labeled motor axons and axon terminals, respectively. Rhodamine-conjugated α-bungarotoxin (Life Technologies) labeled postsynaptic acetylcholine receptors. Diaphragms were then coverslipped with Vectashield mounting medium (Vector Laboratories, Burlingame, CA). Diaphragms were imaged on a FluoView FV1000 confocal microscope (Olympus, Center Valley, PA) and analyzed in a blinded manner for total numbers of intact, denervated and partial denervated NMJs (Wright et al., 2007; Wright et al., 2014; Wright et al., 2009; Wright and Son, 2007). We restricted NMJ analysis to the ipsilateral hemi-diaphragm because no change in denervation or sprouting in contralateral hemi-diaphragm was detected after unilateral cervical contusion SCI in our previous study (Nicaise et al., 2012b).

2.10. Immunohistochemistry

Frozen transverse sections of cervical spinal cord were air-dried and washed three times (5 min each) with PBS. Samples were then incubated in blocking solution (5% normal goat serum and 0.4% Triton X-100 diluted in PBS) for 1 h at room temperature. Sections were incubated overnight at 4 °C with primary antibodies in blocking solution. The following primary antibodies were used: anti-CD68 (1:1000, AbD Serotec) to identify reactive microglia/macrophages, anti-iNOS (1:5000, Millipore) to identify M1 phenotype, anti-arginase 1 (Arg1, 1:500, Santa Cruz Biotechnology) to identify M2 phenotype, and polyclonal rabbit 5-HT antibody (1: 15,000, Immunostar, Hudson, WI). Sections were then washed with PBS (3 washes, 5 min each) and incubated with secondary antibodies conjugated to Alexa fluorophores (1:200, Invitrogen) in blocking solution for 1 h at room temperature. After washing with PBS (3 washes, 5 min each), sections were coverslipped. For 5-HT staining, images were acquired with a Zeiss Imager M2 upright microscope, and MetaMorph software was used to quantify the intensity of 5-HT immunostaining specifically in the ventral horn of sections with CTB-labeled PhMNs. For stereological quantification of the number of $CD68^+$ reactive microglia/macrophages, $iNOS^+/CD68^+$ M1 cells and $Arg1^+/CD68^+$ M2 cells, tissue sections were imaged on a Zeiss AxioObserver Wide Field inverted microscope equipped with Slidebook 6 software. All quantifications were conducted in a blinded manner. The percentages of M1 and M2 microglia/macrophages were determined by dividing the number of $iNOS^+/CD68^+$ (M1) and $Arg1^+/CD68^+$ (M2) cells by number of $CD68^+$ cells (reactive microglia/macrophage), respectively.

2.11. Statistics

Results were expressed as means ± standard error of the mean (SEM). Comparisons between two groups were analyzed using an unpaired *t*-test, and multiple comparisons between three or more groups were analyzed using analysis of variance (one-way ANOVA), followed by post hoc test (Bonferroni's method). Graphpad Prism 5 (GraphPad Software, La Jolla, CA) was used to calculate statistics. $P < .05$ was used as the threshold for statistical significance.

3. Results

3.1. Minocycline hydrogel implantation significantly preserved diaphragm function following cervical contusion SCI

We assessed inspiratory EMGs and evoked CMAPs in order to evaluate the in vivo effects of MH hydrogel implantation on respiratory functional recovery of the diaphragm following SCI. We measured EMG burst amplitude in the ipsilateral hemi-diaphragm during normal, rhythmic breathing to assess diaphragm activation and function. The ventral, medial, and dorsal sub-regions of the diaphragm are innervated by PhMNs, whose cell bodies are predominantly located in cervical regions C3, C4, and C5, respectively (Laskowski and Sanes, 1987); therefore, we recorded EMGs in each sub-region as a measure of diaphragm innervation from each cervical level. In contusion animals that received a blank hydrogel control, we observed a significant decrease in EMG amplitude at all three sub-regions; the most pronounced loss occurred in the dorsal region, which is innervated primarily by PhMNs whose somata are found at C5. Our unilateral contusion injury is located at the C4/C5 level, which may explain the lower EMG burst amplitudes in blank-hydrogel control animals at the dorsal and medial sub-regions. Compared to blank hydrogel (Fig. 1A), MH hydrogel significantly preserved diaphragm EMG amplitudes at 5 weeks post-SCI (Fig. 1B). MH hydrogel exerted a therapeutic effect on EMG amplitude only at the dorsal sub-region (Fig. 1B-C). Our hydrogel was implanted directly above the contusion epicenter, and we found that MH concentration in the lesion epicenter segment was higher than that in the adjacent segments (data not shown). This may explain why MH hydrogel selectively preserved diaphragm EMG amplitudes at the dorsal sub-region. We observed no differences in burst frequency (Fig. 1D) or burst duration (Fig. 1E) between blank hydrogel control and MH hydrogel treatment groups at any sub-region of the hemi-diaphragm; these burst frequency and duration values were similar to previously reported values for uninjured control animals (Li et al., 2015a).

In addition to EMG recordings to measure rhythmic breathing, we also conducted CMAPs to measure evoked diaphragm function. In contrast to spontaneous EMG recordings, CMAPs enable us to assess functional innervation of the diaphragm by PhMNs independent of descending input from the brainstem. We stimulated the phrenic nerve to a supramaximal level, and using a surface electrode, we recorded CMAP amplitudes simultaneously from all three sub-regions of the hemi-diaphragm. We compared CMAP recordings of blank hydrogel and MH hydrogel implanted rats, as well as both the ipsilateral and contralateral hemi-diaphragm in each group (Fig. 2A). We found a significant and persistent increase in peak CMAP amplitudes in the ipsilateral hemi-diaphragm of the MH hydrogel group in comparison to the blank hydrogel group at 1, 2 and 3 weeks post-injury (Fig. 2B). Moreover, compared to the intact contralateral hemi-diaphragm of the same animal, CMAP amplitudes from the ipsilateral hemi-diaphragm of blank hydrogel animals were significantly decreased at all three weeks. In contrast, MH hydrogel rescued CMAP amplitudes in the ipsilateral hemi-diaphragm compared to the contralateral hemi-diaphragm of the same animal (Fig. 2B).

Based on the results of our electrophysiological assessments of diaphragm activation, we found that local delivery of a MH hydrogel at the injury site significantly and persistently protected against

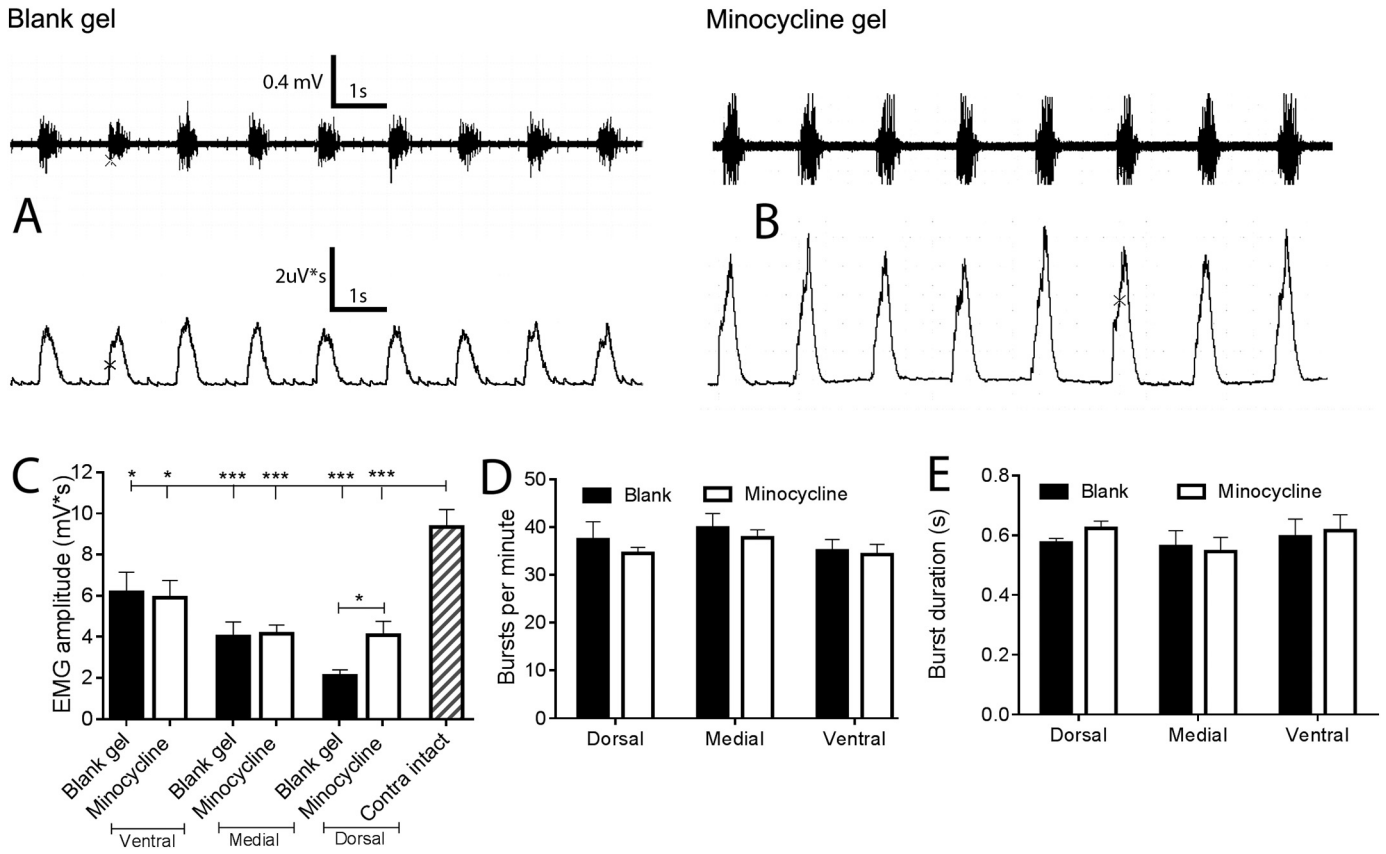

Fig. 1. Minocycline hydrogel preserved diaphragm function following cervical contusion SCI. We recorded EMGs from ipsilateral hemi-diaphragm five weeks after injury and MH hydrogel implantation. Representative raw (upper) and integrated (lower) EMG recordings for blank hydrogel control (A) and MH hydrogel (B) groups. We quantified integrated EMG amplitude (C), burst frequency (D) and burst duration (E). Our results are reported as means ± SEM (n = 6–10 animals per condition). *$p < .05$; ***$p < .001$; ANOVA; MH hydrogel group versus blank hydrogel or experimental group versus contralateral intact. In panel C, all statistical comparisons along the top line of the graph are versus the intact condition, demonstrating that all contusion groups (regardless of treatment) still had lower EMG amplitudes than the intact EMGs.

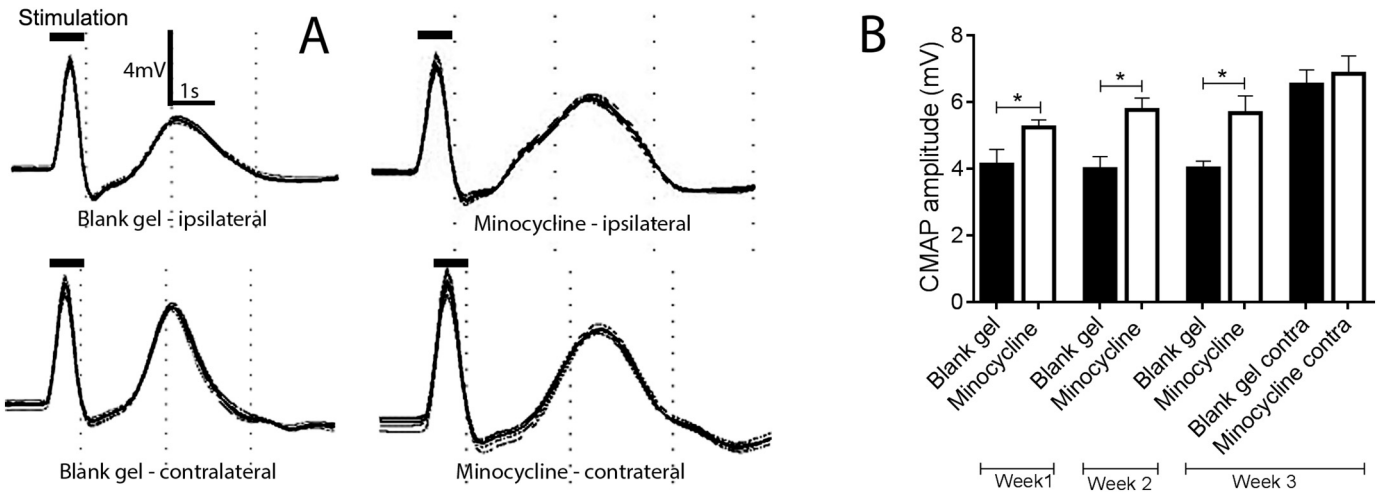

Fig. 2. Minocycline hydrogel preserved functional diaphragm innervation following cervical contusion SCI. We supramaximally stimulated the phrenic nerve and recorded CMAPs from the ipsilateral or contralateral hemi-diaphragm for blank hydrogel control (left traces) and MH hydrogel treatment (right traces) groups (**A**). We quantified CMAP amplitudes at 1, 2, and 3 weeks following injury (**B**). Our results are reported as means ± SEM (n = 4–5 animals per condition). *p < .05; ANOVA; MH hydrogel group versus blank hydrogel.

diaphragm compromise after cervical contusion.

3.2. Minocycline hydrogel decreased lesion size and degeneration of cervical motor neuron cell bodies

We quantified size of the contusion lesion and sparing of motor neurons located in the ventral horn to address whether the improvement in diaphragm function in MH hydrogel animals was due to a central neuroprotective effect in the cervical spinal cord. We used cresyl violet to stain for Nissl bodies in transverse sections of cervical spinal cord tissue. In MH hydrogel animals (Fig. 3D-F), lesion size was significantly reduced compared to blank hydrogel control animals (Fig. 3A-C) both at the lesion epicenter as well as extending up to 1–2 mm rostral and caudal from the epicenter (Fig. 3G). Additionally, using the Cavalieri estimator of volume, we found that MH hydrogel implantation reduced total lesion volume compared to the blank hydrogel controls (Fig. 3H). EMG recovery (in the dorsal sub-region of the ipsilateral hemi-diaphragm) was also correlated with reduced lesion size (Fig. 3I). In addition to cresyl violet analysis, we quantified lesion size using GFAP immunostaining to mark the extent of the lesion. Compared to blank gel (Fig. 3J-L), MH hydrogel (Fig. 3M-O) reduced lesion size in GFAP-labeled sections at multiple rostral-caudal distances from the lesion epicenter (Fig. 3P) and overall lesion volume (Fig. 3Q). These results are consistent with our previous observation in a unilateral C5 contusion injury model (Wang et al., 2017), confirming that local delivery of high concentrations of MH from subdurally implanted hydrogel can significantly reduce tissue damage after cervical contusion SCI.

Compared to blank hydrogel controls (Fig. 4A), MH hydrogel mitigated the loss of motor neuron cell bodies within the ipsilateral ventral horn at 5 weeks following contusion SCI (Fig. 4B). We observed this cervical motor neuron protection at multiple locations both rostral and caudal to the lesion epicenter (Fig. 4C). MH hydrogel also increased the total number of these ipsilateral motor neurons across the entire C3–5 spinal cord (Fig. 4D). Lastly, EMG recovery in the dorsal sub-region of the muscle was correlated with increased numbers of total MNs (Fig. 4E).

The results of our histological analyses suggest that MH hydrogel exerted a central neuroprotective effect in the cervical spinal cord by reducing lesion size and preserving motor neurons post-SCI.

3.3. Minocycline hydrogel preserved PhMN innervation of the diaphragm

In addition to promoting central neuroprotection within the cervical spinal cord, MH hydrogel may have also played a protective role in peripheral innervation at the diaphragm NMJ, where the PhMNs synapse onto the diaphragm to stimulate diaphragmatic activity. Therefore, we delivered the retrograde axonal tracer, Alexa647-conjugated CTB, to the ipsilateral hemi diaphragm via intrapleural injection at four weeks following injury in order to selectively label PhMN cell bodies and assess diaphragm innervation. At this late injection time point post-injury, secondary loss of PhMNs has already occurred (Nicaise et al., 2013) and CTB will only be retrogradely transported to selectively label PhMNs in an intact circuit where the PhMN innervates the muscle. As shown in the sagittal orientation from contusion rats, CTB-labeled PhMNs form a compact, linear column along cervical spinal cord (Fig. 5A-B). Transverse spinal cord sections from contusion animals implanted with blank or MH hydrogel demonstrate that the CTB-labeled PhMNs are located in the ipsilateral ventral horn (Fig. 5C-D). In MH hydrogel animals, we observed a significantly greater number of CTB-labeled PhMNs per section compared to blank hydrogel controls at 1–2 mm rostral to the lesion epicenter (Fig. 5C-E). EMG recovery (in the dorsal diaphragm sub-region) was also correlated with increased numbers of PhMNs at this rostral 1–2 mm location (Fig. 5F). At 0–1 mm rostral to the epicenter, there was complete loss of CTB labeling in both groups and therefore no effect of MH on CTB^+ PhMN numbers. In addition, there were no differences between blank and MH hydrogel groups in average number of CTB-labeled PhMNs per section at 2–3 mm or 3–4 mm rostral to the lesion epicenter, likely because the contusion induced little-to-no PhMN injury at these greater distances from the lesion. These data suggest that MH hydrogel robustly preserved PhMN innervation of the diaphragm.

In order to further evaluate the effects of MH hydrogel on diaphragm innervation, we used confocal imaging to conduct a morphological analysis of individual NMJ synapses in the dorsal, medial and ventral sub-regions of the ipsilateral hemi-diaphragm 5 weeks post-SCI. We performed whole-mount immunohistochemistry on the hemi-diaphragm to label phrenic motor axons with neurofilament (SMI-312) and their terminals with synaptic vesicle protein 2 (SV2) antibodies. Postsynaptic nicotinic acetylcholine receptors were labeled with Alexa555-conjugated α-bungarotoxin. Complete overlap of SV2 + SMI32 with α-bungarotoxin was indicative of a fully innervated synapse. MH hydrogel animals (Fig. 6B) had a significantly greater percentage of fully-

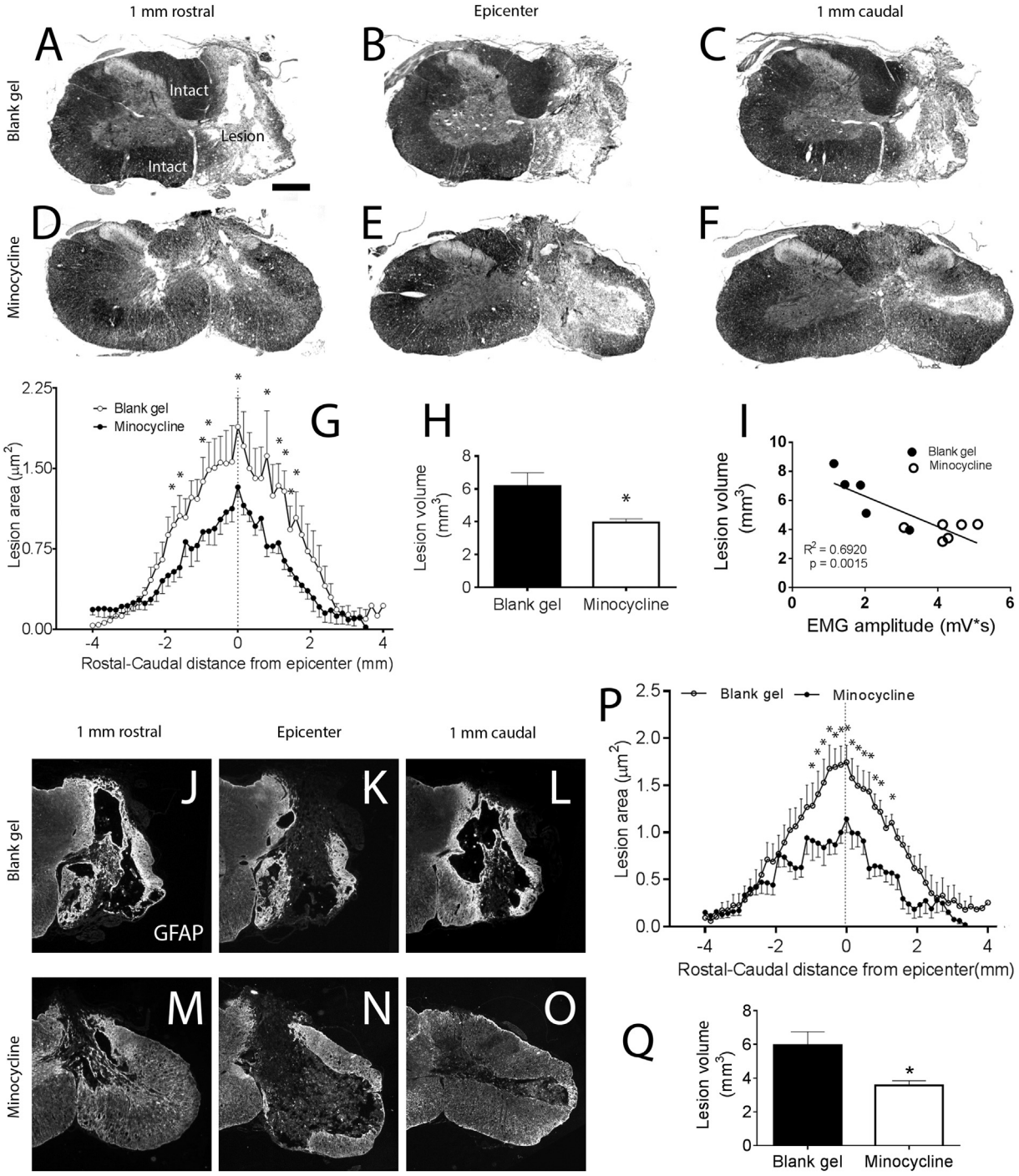

Fig. 3. Minocycline hydrogel reduced lesion size following cervical contusion SCI. At five weeks post-injury, we quantified size of the contusion lesion in transverse sections of the cervical spinal cord following Cresyl-violet staining. Representative images of spinal cord at lesion epicenter, 1 mm rostral to epicenter, and 1 mm caudal to epicenter for blank hydrogel (**A-C**) and MH hydrogel (**D-F**) treated animals. Scale bar, 500 μm. With MH hydrogel treatment, there was a significant decrease in lesion area at multiple rostral-caudal locations (**G**) and in total lesion volume (**H**). EMG recovery (in the dorsal sub-region of the ipsilateral hemi-diaphragm) was also correlated with reduced lesion size (**I**). In addition to cresyl violet analysis, we quantified lesion size using GFAP immunostaining to mark the extent of lesion expansion. Compared to blank gel (**J-L**), MH hydrogel (**M-O**) reduced lesion size in GFAP-labeled sections at multiple rostral-caudal distances form the lesion epicenter (**P**) and overall lesion volume (**Q**). Our results are reported as means ± SEM (n = 4–6 animals per group). *$p < .05$; ANOVA (G); *t*-test (H); MH hydrogel group versus blank hydrogel. (For interpretation of the references to colour in this figure legend, the reader is referred to the web version of this article.)

innervated NMJs (Fig. 6C) in comparison to blank hydrogel animals in the dorsal sub-region (Fig. 6A). Furthermore, MH hydrogel animals had a decreased percentage of both partially-denervated (Fig. 6D) and completely-denervated (Fig. 6E) NMJs in the same sub-region. Our NMJ morphological analysis was consistent with our functional EMG data (Fig. 1C). We observed a lesser degree of diaphragm denervation in the ventral sub-region (which showed the largest EMG amplitudes), while we found the largest amount of denervation in the dorsal sub-region (which had the lowest EMG amplitudes). We also found a smaller degree of denervation in the medial sub-region. These results are likely because the dorsal sub-region is predominantly innervated by PhMNs at C5 that are located closest to the contusion epicenter. MH hydrogel

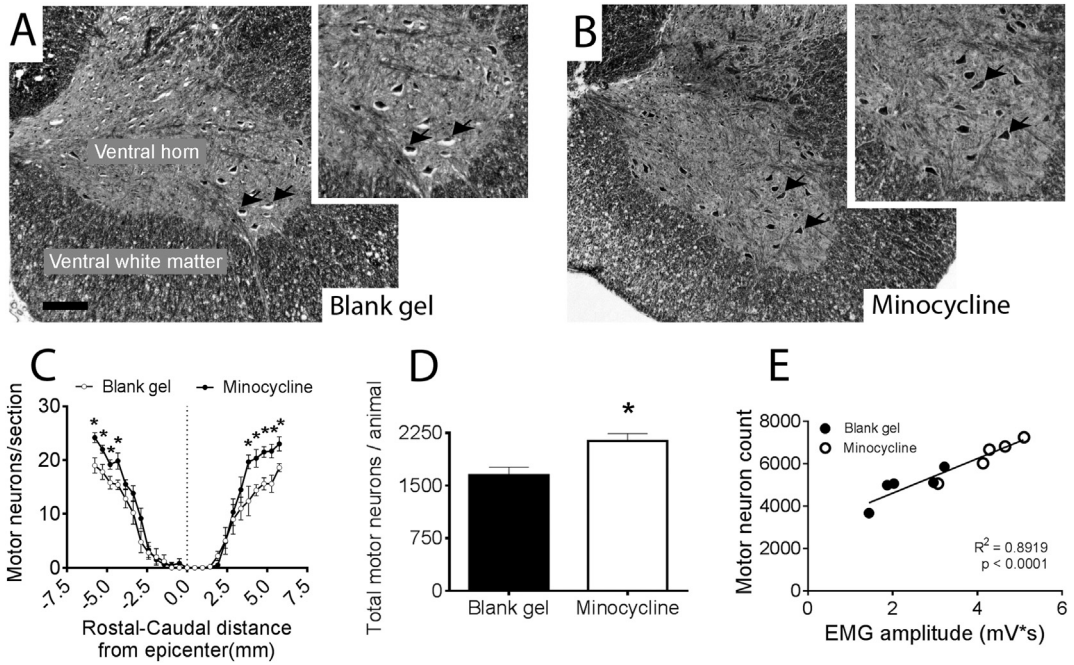

Fig. 4. Minocycline hydrogel reduced degeneration of cervical motor neurons following cervical contusion SCI. Representative images showing motor neuron cell bodies (indicated by arrow in both lower magnification images and higher magnification insets) in ventral horn of the cervical spinal cord of blank hydrogel (**A**) and MH hydrogel (**B**) treated animals. Scale bar, 200 µm. Distribution of motor neuron cell body counts per section at multiple rostral-caudal distances from the epicenter (**C**). Total motor neuron counts from C3-C5 spinal cord (**D**). EMG recovery in the dorsal sub-region of the muscle was correlated with increased numbers of total MNs (**E**). Our results are reported as means ± SEM (n = 4 animals per group). *$p < .05$; ANOVA (C); t-test (D); MH hydrogel group versus blank hydrogel.

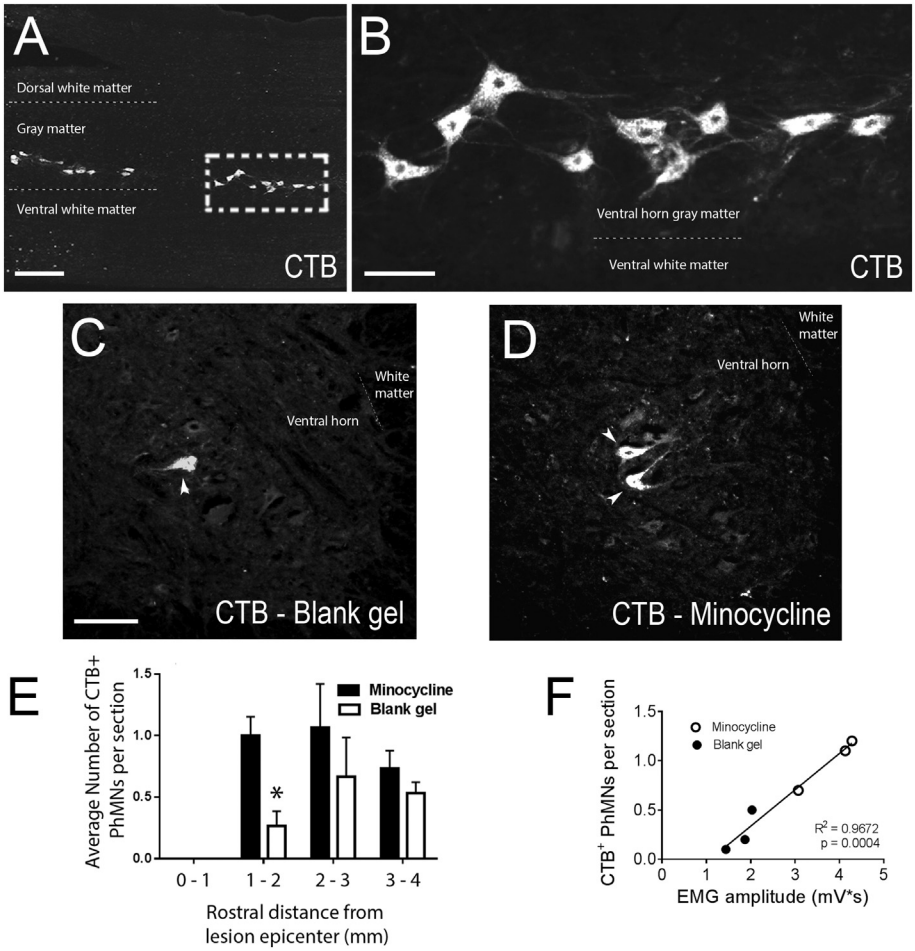

Fig. 5. Minocycline hydrogel preserved number of CTB-labeled PhMNs that innervate the diaphragm following cervical contusion SCI. We intrapleurally injected the retrograde tracer, Alexa647-conjugated CTB, into the ipsilateral hemi-diaphragm to selectively label PhMN cell bodies in the ipsilateral ventral horn of the cervical spinal cord. Sagittal spinal cord sections from contusion animals show a compact, linear column of CTB-labeled PhMNs located in the cervical spinal cord (**A**, higher magnification of outlined area shown in **B**). Transverse sections were used to quantify the number of CTB-labeled PhMNs in the ipsilateral ventral horn (**C-D**). Compared to blank hydrogel controls (C), MH hydrogel animals (D) had significantly greater numbers of CTB-labeled PhMNs per section at 1–2 mm rostral to the lesion epicenter, but no effects of MH were noted at 0–1, 2–3 or 3–4 mm rostral to the epicenter (**E**). EMG recovery (in the dorsal diaphragm sub-region) was correlated with increased numbers of PhMNs at the rostral 1–2 mm location (**F**). Scale bars in A, C-D: 100 µm. Our results are reported as means ± SEM ($n = 3$ animals per group). *$p < .05$; t-test; MH hydrogel versus blank hydrogel.

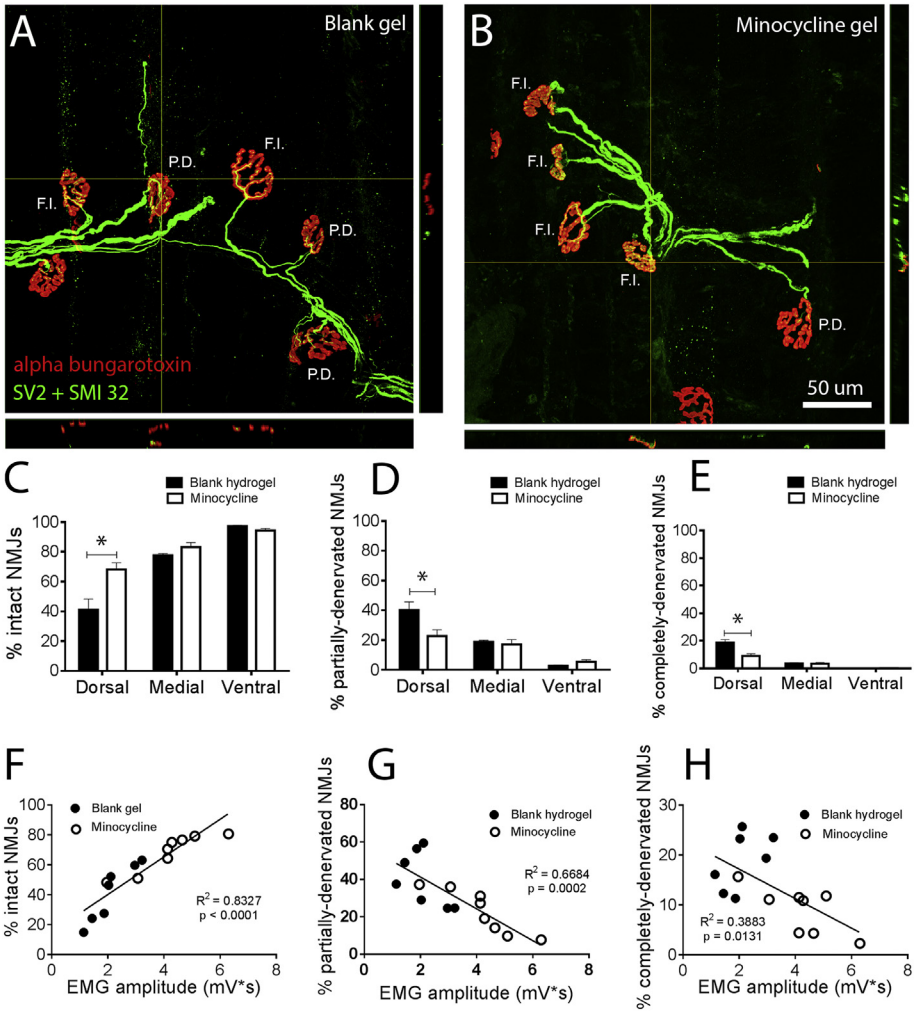

Fig. 6. Minocycline hydrogel preserved phrenic motor neuron innervation of the diaphragm NMJ following cervical contusion SCI. On the ipsilateral hemi-diaphragm, we labeled phrenic motor axons and their terminals with neurofilament (SMI-312) and synaptic vesicle protein 2 (SV2) antibodies, respectively, at five weeks post-SCI using whole-mount immunohistochemistry. Both SMI-312 and SV2 labeling are shown in green. Alexa555-conjugated α-bungarotoxin (red) labeled post-synaptic nicotinic acetylcholine receptors in the diaphragm. In the dorsal sub-region of the muscle, MH hydrogel (**B**) significantly increased the percentage of fully-innervated NMJs (**C**) compared to blank hydrogel (**A**). Panels A-B: F.I. denotes fully-innervated NMJs; P.D. denotes partially-denervated NMJs. MH hydrogel also reduced the percentage of both partially-denervated (**D**) and completely-denervated (**E**) NMJs in the dorsal sub-region. EMG amplitudes in the dorsal sub-region correlated with the degree of intact NMJs in the same dorsal hemi-diaphragm sub-region (**F**), but were inversely correlated with the degree of partial (**G**) and complete (**H**) denervation. Scale bar, 50 μm. Our results are reported as means ± SEM (n = 3 animals per condition). *$p < .05$; ANOVA; MH hydrogel versus blank hydrogel. (For interpretation of the references to colour in this figure legend, the reader is referred to the web version of this article.)

implantation significantly attenuated peripheral NMJ denervation at the dorsal sub-region, which corresponds to the significant preservation of EMG amplitudes at this same location. Lastly, EMG amplitudes in the dorsal sub-region correlated with the degree of intact NMJs in the same dorsal hemi-diaphragm sub-region (Fig. 6F), but were inversely correlated with the degree of partial (Fig. 6G) and complete (Fig. 6H) denervation.

Using retrograde PhMN labeling and NMJ analysis, we found that MH hydrogel significantly preserved diaphragm NMJ innervation by PhMNs, which was consistent with the results of our EMG recordings of diaphragm activity. We have shown that local MH hydrogel treatment protects both motor neuron cell bodies (Fig. 4) and axonal projections (Wang et al., 2017). This may lead to the protection of PhMNs and their axons, and consequently the overall PhMN-diaphragm circuit.

3.4. Minocycline hydrogel was effective in modulating microglia/macrophage response

We next evaluated the microglia/macrophage response at 1 mm rostral to the lesion epicenter as we observed significant neuroprotective effects of MH hydrogel at this location compared to blank hydrogel control (Fig. 3A, D, G). At 5 weeks after SCI, MH hydrogel significantly reduced the number of $CD68^+$ cells compared to blank control (Fig. 7A and B), suggesting that MH hydrogel suppressed the activation of microglia/microphages. We further examined the effect of local MH hydrogel treatment on microglia/macrophage polarization. Fig. 7A and C show that the percentage of $iNOS^+/CD68^+$ cells (denoted as "%M1") was significantly reduced in the MH hydrogel group compared to blank hydrogel, whereas that of $Arg1^+/CD68^+$ cells (%M2) remained unchanged. As a result, M1/M2 ratio was significantly reduced in the MH hydrogel group (Fig. 7D). Furthermore, dorsal hemi-diaphragm EMG amplitudes were correlated with reduced CD68 + cell counts (Fig. 7E), M1 cell percentage (Fig. 7F) and M1/M2 ratio (Fig. 7G).

3.5. Minocycline hydrogel did not enhance serotonergic axon innervation of PhMNs

MH has been shown to decrease axon growth-inhibitory chondroitin sulfate proteoglycans (CSPGs) (Kang et al., 2010) and astrogliosis (Teng et al., 2004) after SCI, possibly because it inhibits the activation of microglia/macrophage and their production of pro-inflammatory cytokines that can activate astrocytes. Therefore, MH could potentially promote repair/regeneration by creating a less inhibitory environment for axon growth. We investigated whether the therapeutic effects of MH hydrogel on diaphragm function occurred via reparative mechanisms in addition to neuroprotection within the spinal cord and preservation of NMJ innervation. It is known that descending serotonergic signaling modulates motor neuron excitability in the spinal cord (Perrier et al., 2013). Along these lines, MH hydrogel may be able to strengthen rhythmic glutamatergic bulbospinal input to PhMNs by increasing serotonergic fiber sprouting and thus increasing excitatory input to PhMNs. To investigate this hypothesis, we immunostained the ipsilateral ventral horn of cervical regions C3–5 for 5-HT at 5 weeks following injury and quantified the intensity of the 5-HT staining. We

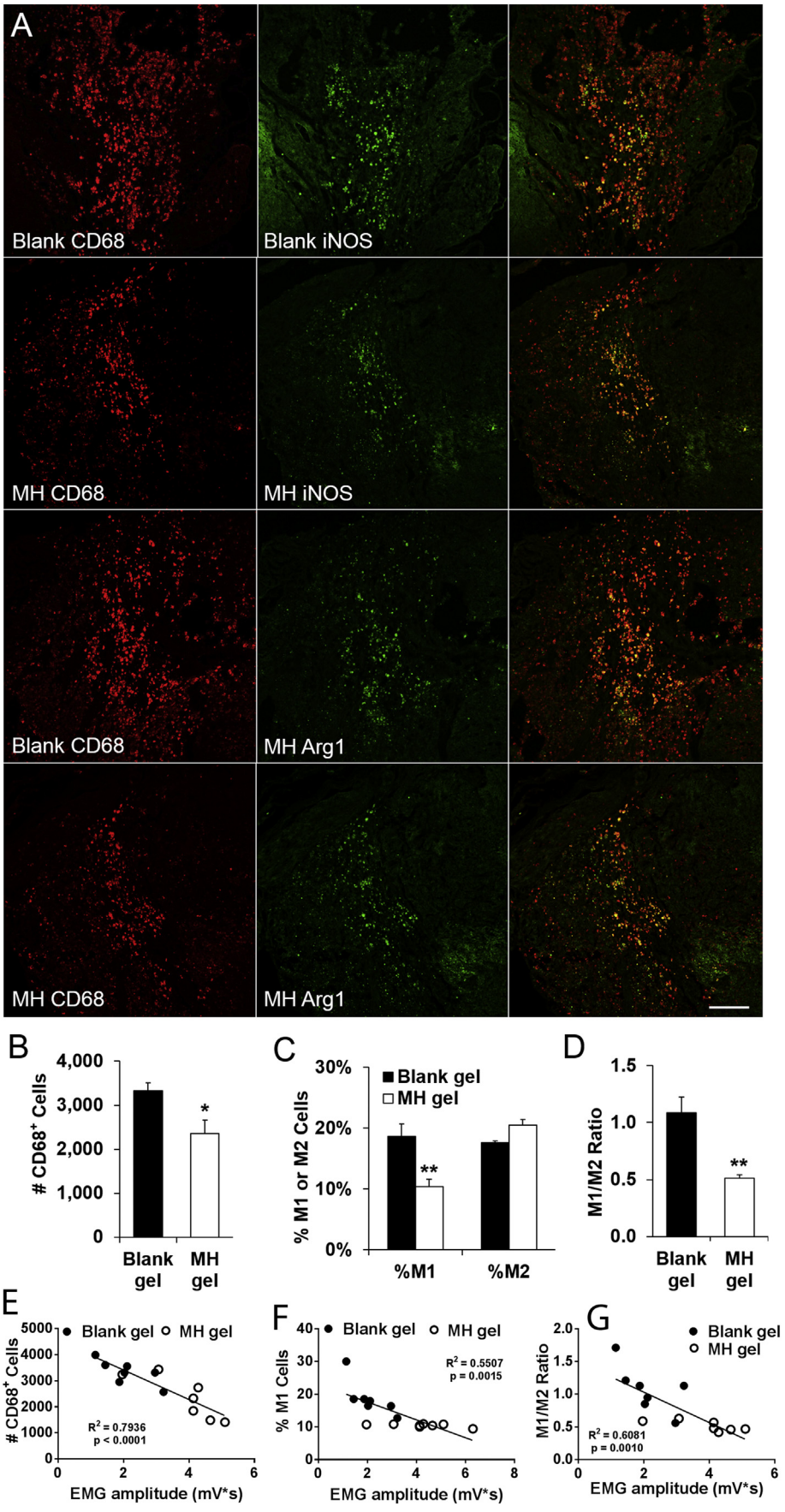

Fig. 7. Minocycline hydrogel reduced reactive microglia/macrophages and inhibited M1 polarization following cervical contusion. At five weeks post-contusion, transverse sections 1 mm rostral to lesion epicenter were double-immunostained for CD68 (red) and iNOS (green) to identify M1 polarization or CD68 (red) and Arg1 (green) to identify M2 polarization. Representative images of $CD68^+$ reactive microglia/macrophages, $iNOS^+$ M1 phenotype and $Arg1^+$ M2 phenotype for blank hydrogel and MH hydrogel treated animals (**A**). Scale bar, 100 μm. With MH hydrogel treatment, there was significant reduction in the number of $CD68^+$ reactive microglia/macrophages (**B**) % M1 cells (no significant change in % M2 cells) (**C**), and M1/M2 ratio (**D**). Dorsal hemi-diaphragm EMG amplitudes were correlated with reduced CD68+ cell counts (**E**), percentage of M1 cells (**F**) and M1/M2 ratio (**G**). We expressed results as means ± SEM ($n = 6$ animals per group). $^*p < .05$, $^{**}p < .01$; *t*-test (B, D); ANOVA (C); MH hydrogel group versus blank hydrogel. (For interpretation of the references to colour in this figure legend, the reader is referred to the web version of this article.)

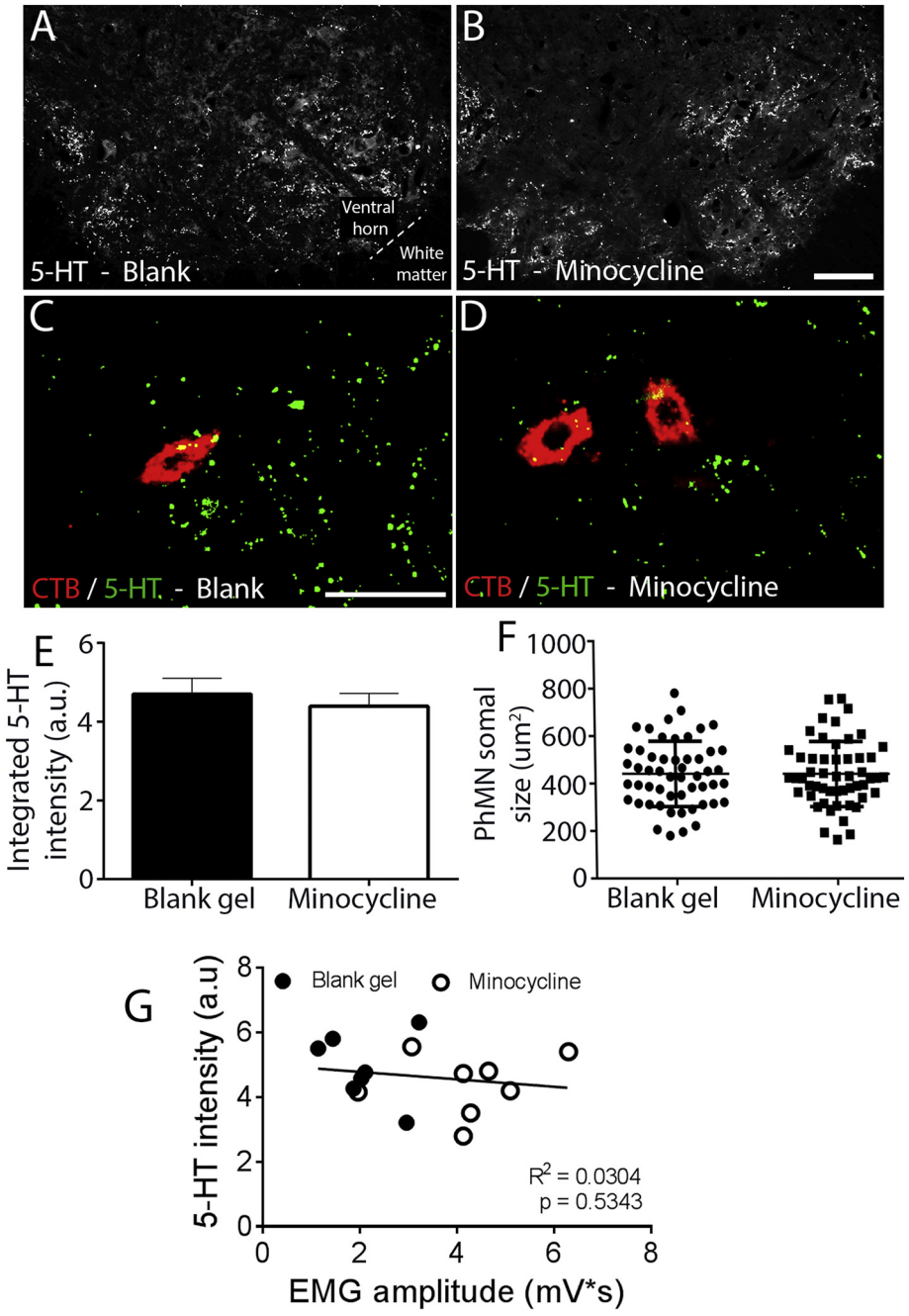

Fig. 8. Minocycline hydrogel did not alter serotonergic axon innervation of PhMNs following cervical contusion. We immunostained for 5-HT in the ipsilateral ventral horn of cervical levels C3–5. At five weeks following contusion injury, in comparison to blank hydrogel controls (**A**, **C**), MH hydrogel (**B**, **D**) did not alter the density of serotonergic fibers directly surrounding PhMNs that had been retrogradely labeled with CTB (**E**). Somal size of CTB-labeled PhMNs in the MH hydrogel group was similar when compared to blank hydrogel control (**F**). There was no correlation between diaphragm functional recovery as determined by EMG amplitudes in the dorsal hemi-diaphragm and 5-HT axon density in the C3–5 ventral horn (**G**). Our results were expressed as means ± SEM (n = 4 animals per group); t-test (E-F).

found that MH hydrogel (Fig. 8B, D) did not increase the density of serotonergic axons surrounding CTB-labeled PhMNs in comparison to blank hydrogel controls (Fig. 8A, C) (quantification in Fig. 8E). In addition, there was no correlation between diaphragm recovery as determined by EMG amplitudes in the dorsal hemi-diaphragm and 5-HT axon density in the C3–5 ventral horn (Fig. 8G). Therefore, MH hydrogel did not promote serotonergic axon plasticity surrounding the location of the PhMNs in the cervical spinal cord and likely did not alter descending input that modulates PhMN excitability. We also tested whether MH hydrogel implantation exerted effects on the cell body size of CTB-labeled PhMN, as neuronal excitability is associated with somal size. We found no alteration of PhMN cell body size between blank hydrogel and MH hydrogel (Fig. 8F). Given these findings, it is likely that local MH hydrogel delivery to the injured cervical spinal cord improved respiratory function via protecting rather than repairing the neural circuitry that controls diaphragm activation.

4. Discussion

4.1. Summary of findings and conclusions

High concentrations of MH can potentially target multiple secondary injury mechanisms after SCI. In a clinically relevant animal model of cervical contusion SCI, we show that local delivery of high MH concentrations from a hydrogel-based drug delivery system effectively preserved diaphragmatic respiratory function by protecting the important neural circuitry that controls diaphragm activation. Specifically, MH hydrogel decreased lesion size and degeneration of cervical motor neuron somata. Furthermore, MH hydrogel significantly preserved diaphragm innervation by the axons of PhMNs, as evidenced by increased intact NMJs and CTB-retrograde labeled PhMNs. Moreover, MH hydrogel significantly reduced microglia/macrophage activation and selectively inhibited M1 polarization, which may also

contribute to the neuroprotective effects of MH. On the other hand, minocycline hydrogel did not enhance serotonergic axon innervation of PhMNs, suggesting that its therapeutic mechanism of action was not via neural repair/regeneration, though we tested only this one form of axonal plasticity. In conclusion, our findings demonstrate that local MH hydrogel delivery to the injured cervical spinal cord is an effective strategy for preserving respiratory function after SCI.

4.2. Neuroprotective effects of MH hydrogel on respiratory neural circuitry

Together, our histological findings of decreased lesion size and degeneration of cervical motor neuron cell bodies demonstrate that MH hydrogel exerted robust neuroprotective effects within the injured cervical spinal cord. Studies have shown that MH is fully neuroprotective at a concentration range of 35–75 μg/mL (Kraus et al., 2005) (Wang et al., 2003) (Garcia-Martinez et al., 2010) (Xue et al., 2010). Our previous study showed that the current MH hydrogel formulation can deliver 35.7 to 24.7 μg/mL from day 1 to 3 in the local spinal cord tissue (Wang et al., 2017). Therefore, local MH concentration starting from day-2 post-injury may not have been sufficiently high to target some secondary injury mechanisms effectively. In addition, studies have shown that tissue loss extends out to approximately 7 days after SCI, with apoptosis of certain cell lineages occurring beyond this point (Liu et al., 1997; Ek et al., 2010). Therefore, further optimization of the drug delivery system to achieve high doses of MH release for at least 7 days (or longer) may be even more effective in reducing tissue damage and cell loss.

Compared to the blank hydrogel group, MH hydrogel was more effective in preserving total CTB counts across the PhMN pool (by 202%; data not shown) than protection of all motor neuron somata in the cresyl violet analysis (by 30%; Fig. 4D). For quantification in cresyl violet-stained tissue, we counted all motor neurons with intact cell bodies. However, the neural circuitry into which some of these neurons are integrated may be disrupted because of axonal damage/loss or synaptic disconnection. In contrast, for PhMN quantification only the neurons with intact PhMN-diaphragm synaptic connection can be labeled and counted using CTB. Therefore, the more pronounced protective effect of MH hydrogel on total CTB counts than total motor neuron counts suggests that MH also strongly preserved the entire PhMN-to-diaphragm portion of the respiratory circuit beyond effects on just cell body protection. This result is not surprising, as we previously showed that MH hydrogel significantly preserved myelinated axons centrally within the spinal cord compared to blank hydrogel control (Wang et al., 2017).

While our findings do support the notion that MH preserved diaphragm function via neuroprotective effects on respiratory circuitry, we do not provide causal data to directly establish this conclusion. We did conduct correlation analyses that show on an individual animal basis that diaphragm functional recovery was significantly correlated with reduced lesion size, increased numbers of total MNs and PhMNs, the degree of morphological NMJ innervation, and reduction in the intraspinal pro-inflammatory response, supporting that local MH delivery was indeed acting via a neuroprotective mechanism.

4.3. Temporal considerations for targeting the PhMN-diaphragm circuit

To date, studies have not shown PhMN loss beyond the first 24 h post-injury in mid-cervical contusion animal models. Specifically, we previously quantified PhMN loss at days 1, 4, 8 and 14 post-injury in this SCI model and found no additional loss of PhMNs after day-1 (Nicaise et al., 2013). Nevertheless, while we and other groups have not assessed the early time course (i.e. within the first 24 h) of PhMN soma loss or lesion expansion in mid-cervical contusion SCI models, we do show in the current study that acute delivery of MH hydrogel can decrease PhMN loss, regardless of when it occurs. Our proof-of-principle study suggests that early manipulation using MH can impact PhMN survival, which, given our previous CTB time-course data, is likely mediated through effects on events occurring only during the first day post-injury.

In addition to PhMN protection, we find a significant effect on preservation of diaphragm innervation by phrenic motor axons using NMJ morphological analysis; therefore, our approach is not only restricted to central protection of PhMN cell bodies within the cervical spinal cord. Unlike with our time-course analysis of PhMN somal loss, we previously reported a progressive decrease in morphological innervation at the diaphragm NMJ following mid-cervical contusion from 1 to 14 days post-injury (Nicaise et al., 2013). This longer window may allow for therapeutic benefit of MH delivery even when hydrogel is implanted with a delay.

Of relevance to the PhMN counts in both the current study and in our previous work, the timing of intra-diaphragm CTB injection differed; in the current experiment, we injected CTB several weeks after contusion, while we delivered CTB 10 days before to the contusion in our prior study (Nicaise et al., 2013). As retrograde labeling of PhMN somata by CTB injected into the diaphragm requires muscle innervation by the terminals of phrenic motor axons, there are interpretational challenges with directly comparing the results of these two studies. Importantly, CTB injection prior to injury labels all of the PhMN cell bodies, regardless of their diaphragm innervation state at the time of sacrifice and counting, while PhMN somal counts may be confounded by CTB injection performed after injury if a subset of PhMNs have survived the injured but their axons are not innervating the diaphragm. Give this technical issue, the effect of MH hydrogel on CTB counts may have been partly (or even completely) based on changes in peripheral innervation of the diaphragm NMJ by phrenic motor axons and not via PhMN somal protection. Our current data also show significant preservation of NMJ innervation morphologically, which would be in line with the peripheral preservation interpretation of the CTB counts, though these findings do not rule out a simultaneous impact on motor neuron cell body protection within the spinal cord.

With respect to lesion size, we have previously shown progressive lesion expansion from day-1 to day-14 in our unilateral cervical contusion model (Nicaise et al., 2013). Similar to PhMN loss, we have not conducted this lesion analysis during the first 24 h post-injury; nonetheless, our MH hydrogel neuroprotective approach is still relevant given that the lesion continues to expand even beyond day-1 after injury (similar to the progressive denervation at the diaphragm NMJ discussed above), thereby providing an extended time window during which to intervene.

4.4. Therapeutic relevance of findings

In order to study diaphragmatic respiratory dysfunction in a manner that is applicable to the human condition, it is critical to consider the model system. A number of studies have examined respiratory outcome in rodent paradigms of high-cervical (C2) hemisection (Mantilla et al., 2013; Urban et al., 2018) and mid-cervical unilateral (Choi et al., 2005; Nicaise et al., 2012a; Nicaise et al., 2012b) (or midline (Lane et al., 2012)) contusion SCI. Of note, the studies focused on cervical contusion resulted, in general, in modest-to-absent (and relatively-transient) physiological effects on actual ventilatory behavior under normal eupneic conditions, as assessed by whole-body plethysmography. Furthermore, exposing cervical contusion animals to respiratory challenge (e.g. hypercapnia) was often necessary to observe compromised ventilatory function (Choi et al., 2005), though such deficits were not noted in all models (Choi et al., 2005) and diaphragmatic compromise appeared to depend, at least in part, on factors such as the degree of white matter degeneration, likely given the necessity of bulbospinal axon drive to the PhMN pool to achieve diaphragm activation.

Given this collective body of work (including our studies), in the current study we used a unilateral contusion at level C4/5 that resulted in significant - though partial - loss of PhMNs, degeneration of phrenic

motor axons and diaphragm NMJ denervation. We conducted electrophysiological recordings (i.e. EMGs and CMAPs) to specifically assess effects on diaphragm activation and PhMN-diaphragm circuitry (Nicaise et al., 2012a; Nicaise et al., 2012b), though EMGs and CMAPs do not fully provide evaluation of the physiological effects on respiratory function. Importantly, we did not perform assessments of overall ventilatory function such as plethysmography or blood gas measurements (Nicaise et al., 2013). In addition, we did not conduct EMG recordings in response to hypercapic and hypoxic challenges as in some of the previously published studies using similar cervical contusion models. To further examine the therapeutic potential of our MH hydrogel approach, in future work we will need to test effects on these additional functional outcomes and in response to respiratory challenges, in addition to implanting the hydrogel with various delays post-injury that are relevant to clinical translation. That being said, our data do support the potential benefit both of high-dose local MH delivery for preserving this critical neural circuitry and of our novel MH-hydrogel delivery system. Lastly, the therapeutic effects that we have achieved with MH hydrogel only partially improved diaphragm electrophysiological outcome measures; therefore, combination with approaches targeting other disease mechanisms will likely be necessary to further enhance efficacy.

4.5. Modulation of microglia/macrophage response

Macrophages are plastic and adopt dynamic phenotypic and functional properties in response to environmental stimuli (Stout and Suttles, 2004). The pro-inflammatory environment produced by SCI potentiates pathological, neurotoxic microglia/macrophage activation, also called “M1” or classical activation (Kigerl et al., 2009; Kroner et al., 2014; Wang et al., 2015). Following SCI, the potentially reparative and immunosuppressive M2 microglia/macrophage activation (alternative activation) decreases over time, while pathological M1 activation remains elevated (Kigerl et al., 2009) (Kroner et al., 2014; Wang et al., 2015). As a potent anti-inflammatory agent, MH has been shown to reduce inflammation after SCI (Teng et al., 2004; Lee et al., 2003; Wang et al., 2017). Moreover, it has been shown to selectively inhibit M1 polarization of microglia in vitro and in the SOD1-G93A mouse model of amyotrophic lateral sclerosis (ALS) in vivo (Kobayashi et al., 2013). In the context of SCI, we previously found that only local (but not systemic) delivery of MH inhibited M1 microglia/macrophage polarization 6 weeks after unilateral C5 contusion (Wang et al., 2017). On the other hand, the impact force used in our previous work (200 kDyne) was much lower than that used in the present study (395 kDyne). A more severe tissue injury can lead to a stronger inflammatory response. Therefore, in the current study, we examined whether MH can still reduce inflammation and modulate microglia/macrophage polarization in the more severe SCI model. Our data suggest that local MH gel treatment has the same modulatory effect on microglia/macrophage activation and polarization in both modest and severe cervical contusion injuries. MH has been shown to inhibit iNOS activation (Amin et al., 1996; Zhang et al., 2014) and production of pro-inflammatory cytokines including TNFa, IL-1β, and IL-6 (Lee et al., 2003; Kobayashi et al., 2013; Pang et al., 2012), all of which are M1 markers. Therefore, it is not surprising that MH can inhibit M1 polarization. Persistent M1 and transient M2 microglia/macrophage response after SCI leads to enhanced neurotoxicity and impaired wound heading following SCI (Kigerl et al., 2009; Wang et al., 2015). A study showed that for successfully healing diabetic ulcers, M1/M2 ratio started to decrease at 2 weeks and remained low at 3–4 weeks, whereas for non-healing ulcers a high M1/M2 ratio continued increasing over time through 4 weeks (Nassiri et al., 2015). Therefore, the reduced M1/M2 ratio may contribute to the neuroprotective effect of MH. On the other hand, MH hydrogel treatment did not significantly change M2 polarization. Because M2 phenotype is immunomodulatory and is involved in repair and regeneration after SCI (Kigerl et al., 2009; Kroner et al., 2014), it is possible that simultaneously inhibiting M1 and enhancing M2 polarization will be more effective in promoting a normal wound healing response and functional recovery after SCI. It is important to note that we used only immunohistochemistry to study the inflammatory response by assessing expression of a small set of proteins; therefore, it will be critical in future work to more comprehensively address this issue of immunomodulation by MH hydrogel using additional markers and other measures such as flow cytometry.

4.6. MH hydrogel effects on serotonergic axons

Our results show that MH hydrogel did not promote serotonergic axon plasticity within the cervical spinal cord that is associated with modulating PhMN excitability. We also tested whether MH hydrogel implantation exerted effects on the cell body size of CTB-labeled PhMNs, as neuronal excitability is associated with somal size. We found no alteration of cell body size between blank hydrogel and MH hydrogel (Fig. 8F). Given these findings, it is likely that local MH hydrogel delivery to the injured cervical spinal cord improved respiratory function via protecting rather than repairing the neural circuitry that controls diaphragm activation. Following SCI, axons fail to mount a regenerative response due to both a diminished neuronal-intrinsic growth potential and the axon growth inhibitory environment of injured spinal cord, thereby limiting functional recovery (Bradbury and McMahon, 2006). Studies have shown, for example, that combined application of chondroitinase ABC and neurotrophin-3 (NT-3) was more effective in promoting axon regeneration than each individual treatment (Massey et al., 2008; Lee et al., 2010). These studies suggest that it is important to target both the axon growth inhibitory environment and the poor intrinsic regeneration potential to effectively promote regeneration after SCI. We previously showed that local brain-derived neurotrophic factor (BDNF) delivery using a similar engineered hydrogel promoted serotonergic axon growth (Ghosh et al., 2018). Therefore, combined local delivery of both MH (which may be able to reduce environment growth inhibition by modulating the pro-inflammatory macrophage response and by decreasing CSPG levels) and BDNF using our hydrogel approaches may be more effective than BDNF alone or MH alone in promoting the repair of respiratory neural circuitry.

Acknowledgements

This work was supported by the National Institutes of Health (2R01NS079702-06 to A.C.L.), the Craig H. Neilsen Foundation (grant 476686 to A.C.L.), the Margaret Q. Landenberger Research Foundation (to Y.Z.), and the Pennsylvania Tobacco-Commonwealth Universal Research Enhancement (CURE) Research Program (to Y.Z.).

Conflict of interest

The authors declare no competing financial or other interests.

References

Amin, A.R., Attur, M.G., Thakker, G.D., Patel, P.D., Vyas, P.R., Patel, R.N., Patel, I.R., Abramson, S.B., 1996. A novel mechanism of action of tetracyclines: effects on nitric oxide synthases. Proc. Natl. Acad. Sci. U. S. A. 93 (24), 14014–14019.

Bradbury, E.J., McMahon, S.B., 2006. Spinal cord repair strategies: why do they work? Nat. Rev. Neurosci. 7 (8), 644–653.

Casha, S., Zygun, D., McGowan, M.D., Bains, I., Yong, V.W., Hurlbert, R.J., 2012. Results of a phase II placebo-controlled randomized trial of minocycline in acute spinal cord injury. Brain 135 (Pt 4), 1224–1236.

Choi, H., Liao, W.L., Newton, K.M., Onario, R.C., King, A.M., Desilets, F.C., Woodard, E.J., Eichler, M.E., Frontera, W.R., Sabharwal, S., Teng, Y.D., 2005. Respiratory abnormalities resulting from midcervical spinal cord injury and their reversal by serotonin 1A agonists in conscious rats. J. Neurosci. 25 (18), 4550–4559.

Ek, C.J., Habgood, M.D., Callaway, J.K., Dennis, R., Dziegielewska, K.M., Johansson, P.A., Potter, A., Wheaton, B., Saunders, N.R., 2010. Spatio-temporal progression of grey and white matter damage following contusion injury in rat spinal cord. PLoS One 5 (8), e12021.

Garcia-Martinez, E.M., Sanz-Blasco, S., Karachitos, A., Bandez, M.J., Fernandez-Gomez, F.J., Perez-Alvarez, S., de Mera, R.M., Jordan, M.J., Aguirre, N., Galindo, M.F., Villalobos, C., Navarro, A., Kmita, H., Jordan, J., 2010. Mitochondria and calcium flux as targets of neuroprotection caused by minocycline in cerebellar granule cells. Biochem. Pharmacol. 79 (2), 239–250.

Garrido-Mesa, N., Zarzuelo, A., Galvez, J., 2013. Minocycline: far beyond an antibiotic. Br. J. Pharmacol. 169 (2), 337–352.

Ghosh, B., Wang, Z., Nong, J., Urban, M.W., Zhang, Z., Trovillion, V.A., Wright, M.C., Zhong, Y., Lepore, A.C., 2018. Local BDNF delivery to the injured cervical spinal cord using an engineered hydrogel enhances diaphragmatic respiratory function. J. Neurosci. 38 (26), 5982–5995.

Hulsebosch, C.E., 2002. Recent advances in pathophysiology and treatment of spinal cord injury. Adv. Physiol. Educ. 26 (1–4), 238–255.

Kang, Y.M., Hwang, D.H., Kim, B.G., Go, D.H., Park, K.D., 2010. Thermosensitive polymer-based hydrogel mixed with the anti-inflammatory agent minocycline induces axonal regeneration in hemisected spinal cord. Macromol. Res. 18 (4), 399–403.

Kigerl, K.A., Gensel, J.C., Ankeny, D.P., Alexander, J.K., Donnelly, D.J., Popovich, P.G., 2009. Identification of two distinct macrophage subsets with divergent effects causing either neurotoxicity or regeneration in the injured mouse spinal cord. J. Neurosci. 29 (43), 13435–13444.

Kim, H.S., Suh, Y.H., 2009. Minocycline and neurodegenerative diseases. Behav. Brain Res. 196 (2), 168–179.

Kobayashi, K., Imagama, S., Ohgomori, T., Hirano, K., Uchimura, K., Sakamoto, K., Hirakawa, A., Takeuchi, H., Suzumura, A., Ishiguro, N., Kadomatsu, K., 2013. Minocycline selectively inhibits M1 polarization of microglia. Cell Death Dis. 4, e525.

Komai, H., Naito, Y., Okamura, Y., 2005. Dextran sulfate as a leukocyte-endothelium adhesion molecule inhibitor of lung injury in pediatric open-heart surgery. Perfusion 20 (2), 77–82.

Kraus, R.L., Pasieczny, R., Lariosa-Willingham, K., Turner, M.S., Jiang, A., Trauger, J.W., 2005. Antioxidant properties of minocycline: neuroprotection in an oxidative stress assay and direct radical-scavenging activity. J. Neurochem. 94 (3), 819–827.

Kroner, A., Greenhalgh, A.D., Zarruk, J.G., Passos Dos Santos, R., Gaestel, M., David, S., 2014. TNF and increased intracellular iron alter macrophage polarization to a detrimental M1 phenotype in the injured spinal cord. Neuron 83 (5), 1098–1116.

Kwon, B.K., Okon, E., Hillyer, J., Mann, C., Baptiste, D., Weaver, L.C., Fehlings, M.G., Tetzlaff, W., 2011. A systematic review of non-invasive pharmacologic neuroprotective treatments for acute spinal cord injury. J. Neurotrauma 28 (8), 1545–1588.

Lane, M.A., Fuller, D.D., White, T.E., Reier, P.J., 2008. Respiratory neuroplasticity and cervical spinal cord injury: translational perspectives. Trends Neurosci. 31 (10), 538–547.

Lane, M.A., Lee, K.Z., Salazar, K., O'Steen, B.E., Bloom, D.C., Fuller, D.D., Reier, P.J., 2012. Respiratory function following bilateral mid-cervical contusion injury in the adult rat. Exp. Neurol. 235 (1), 197–210.

Laskowski, M.B., Sanes, J.R., 1987. Topographic mapping of motor pools onto skeletal muscles. J. Neurosci. 7 (1), 252–260.

Lee, S.M., Yune, T.Y., Kim, S.J., Park, D.W., Lee, Y.K., Kim, Y.C., Oh, Y.J., Markelonis, G.J., Oh, T.H., 2003. Minocycline reduces cell death and improves functional recovery after traumatic spinal cord injury in the rat. J. Neurotrauma 20 (10), 1017–1027.

Lee, H., McKeon, R.J., Bellamkonda, R.V., 2010. Sustained delivery of thermostabilized chABC enhances axonal sprouting and functional recovery after spinal cord injury. Proc. Natl. Acad. Sci. U. S. A. 107 (8), 3340–3345.

Lepore, A.C., Rauck, B., Dejea, C., Pardo, A.C., Rao, M.S., Rothstein, J.D., Maragakis, N.J., 2008. Focal transplantation-based astrocyte replacement is neuroprotective in a model of motor neuron disease. Nat. Neurosci. 11 (11), 1294–1301.

Lepore, A.C., Tolmie, C., O'Donnell, J., Wright, M.C., Dejea, C., Rauck, B., Hoke, A., Ignagni, A.R., Onders, R.P., Maragakis, N.J., 2010. Peripheral hyperstimulation alters site of disease onset and course in SOD1 rats. Neurobiol. Dis. 39 (3), 252–264.

Li, K., Nicaise, C., Sannie, D., Hala, T.J., Javed, E., Parker, J.L., Putatunda, R., Regan, K.A., Suain, V., Brion, J.P., Rhoderick, F., Wright, M.C., Poulsen, D.J., Lepore, A.C., 2014. Overexpression of the astrocyte glutamate transporter GLT1 exacerbates phrenic motor neuron degeneration, diaphragm compromise, and forelimb motor dysfunction following cervical contusion spinal cord injury. J. Neurosci. 34 (22), 7622–7638.

Li, K., Javed, E., Hala, T.J., Sannie, D., Regan, K.A., Maragakis, N.J., Wright, M.C., Poulsen, D.J., Lepore, A.C., 2015a. Transplantation of glial progenitors that overexpress glutamate transporter GLT1 preserves diaphragm function following cervical SCI. Mol. Ther. 23 (3), 533–548.

Li, K., Javed, E., Scura, D., Hala, T.J., Seetharam, S., Falnikar, A., Richard, J.P., Chorath, A., Maragakis, N.J., Wright, M.C., Lepore, A.C., 2015b. Human iPS cell-derived astrocyte transplants preserve respiratory function after spinal cord injury. Exp. Neurol. 271, 479–492.

Liu, X.Z., Xu, X.M., Hu, R., Du, C., Zhang, S.X., McDonald, J.W., Dong, H.X., Wu, Y.J., Fan, G.S., Jacquin, M.F., Hsu, C.Y., Choi, D.W., 1997. Neuronal and glial apoptosis after traumatic spinal cord injury. J. Neurosci. 17 (14), 5395–5406.

Mantilla, C.B., Gransee, H.M., Zhan, W.Z., Sieck, G.C., 2013. Motoneuron BDNF/TrkB signaling enhances functional recovery after cervical spinal cord injury. Exp. Neurol. 247, 101–109.

Massey, J.M., Amps, J., Viapiano, M.S., Matthews, R.T., Wagoner, M.R., Whitaker, C.M., Alilain, W., Yonkof, A.L., Khalyfa, A., Cooper, N.G., Silver, J., Onifer, S.M., 2008. Increased chondroitin sulfate proteoglycan expression in denervated brainstem targets following spinal cord injury creates a barrier to axonal regeneration overcome by chondroitinase ABC and neurotrophin-3. Exp. Neurol. 209 (2), 426–445.

Nagoshi, N., Fehlings, M.G., 2015. Investigational drugs for the treatment of spinal cord injury: review of preclinical studies and evaluation of clinical trials from phase I to II. Expert Opin. Investig. Drugs 24 (5), 645–658.

Nassiri, S., Zakeri, I., Weingarten, M.S., Spiller, K.L., 2015. Relative expression of Proinflammatory and Antiinflammatory genes reveals differences between healing and nonhealing human chronic diabetic foot ulcers. J Invest Dermatol 135 (6), 1700–1703.

Neimert-Andersson, T., Binnmyr, J., Enoksson, M., Langeback, J., Zettergren, L., Hallgren, A.C., Franzen, H., Lind Enoksson, S., Lafolie, P., Lindberg, A., Al-Tawil, N., Andersson, M., Singer, P., Gronlund, H., Gafvelin, G., 2014. Evaluation of safety and efficacy as an adjuvant for the chitosan-based vaccine delivery vehicle ViscoGel in a single-blind randomised phase I/IIa clinical trial. Vaccine 32 (45), 5967–5974.

Nicaise, C., Hala, T.J., Frank, D.M., Parker, J.L., Authelet, M., Leroy, K., Brion, J.P., Wright, M.C., Lepore, A.C., 2012a. Phrenic motor neuron degeneration compromises phrenic axonal circuitry and diaphragm activity in a unilateral cervical contusion model of spinal cord injury. Exp. Neurol. 235 (2), 539–552.

Nicaise, C., Putatunda, R., Hala, T.J., Regan, K.A., Frank, D.M., Brion, J.P., Leroy, K., Pochet, R., Wright, M.C., Lepore, A.C., 2012b. Degeneration of phrenic motor neurons induces long-term diaphragm deficits following mid-cervical spinal contusion in mice. J. Neurotrauma 29 (18), 2748–2760.

Nicaise, C., Frank, D.M., Hala, T.J., Authelet, M., Pochet, R., Adriaens, D., Brion, J.P., Wright, M.C., Lepore, A.C., 2013. Early phrenic motor neuron loss and transient respiratory abnormalities after unilateral cervical spinal cord contusion. J. Neurotrauma 30 (12), 1092–1099.

Nobunaga, A.I., Go, B.K., Karunas, R.B., 1999. Recent demographic and injury trends in people served by the model spinal cord injury care systems. Arch. Phys. Med. Rehabil. 80 (11), 1372–1382.

Oyinbo, C.A., 2011. Secondary injury mechanisms in traumatic spinal cord injury: a nugget of this multiply cascade. Acta Neurobiol. Exp. (Wars) 71 (2), 281–299.

Pang, T., Wang, J., Benicky, J., Saavedra, J.M., 2012. Minocycline ameliorates LPS-induced inflammation in human monocytes by novel mechanisms including LOX-1, Nur77 and LITAF inhibition. Biochim. Biophys. Acta 1820 (4), 503–510.

Perrier, J.F., Rasmussen, H.B., Christensen, R.K., Petersen, A.V., 2013. Modulation of the intrinsic properties of motoneurons by serotonin. Curr. Pharm. Des. 19 (24), 4371–4384.

Pi, R., Li, W., Lee, N.T., Chan, H.H., Pu, Y., Chan, L.N., Sucher, N.J., Chang, D.C., Li, M., Han, Y., 2004. Minocycline prevents glutamate-induced apoptosis of cerebellar granule neurons by differential regulation of p38 and Akt pathways. J. Neurochem. 91 (5), 1219–1230.

Scarano, A., Carinci, F., Piattelli, A., 2009. Lip augmentation with a new filler (agarose gel): a 3-year follow-up study. Oral Surg. Oral Med. Oral Pathol. Oral Radiol. Endod. 108 (2), e11–e15.

Shanmuganathan, K., Gullapalli, R.P., Zhuo, J., Mirvis, S.E., 2008. Diffusion tensor MR imaging in cervical spine trauma. AJNR Am. J. Neuroradiol. 29 (4), 655–659.

Shoichet, M.S., Tator, C.H., Poon, P., Kang, C., Baumann, M.D., 2007. Intrathecal drug delivery strategy is safe and efficacious for localized delivery to the spinal cord. Prog. Brain Res. 161, 385–392.

Shultz, R.B., Zhong, Y., 2017. Minocycline targets multiple secondary injury mechanisms in traumatic spinal cord injury. Neural Regen. Res. 12 (5), 702–713.

Stirling, D.P., Khodarahmi, K., Liu, J., McPhail, L.T., McBride, C.B., Steeves, J.D., Ramer, M.S., Tetzlaff, W., 2004. Minocycline treatment reduces delayed oligodendrocyte death, attenuates axonal dieback, and improves functional outcome after spinal cord injury. J. Neurosci. 24 (9), 2182–2190.

Stirling, D.P., Koochesfahani, K.M., Steeves, J.D., Tetzlaff, W., 2005. Minocycline as a neuroprotective agent. Neuroscientist 11 (4), 308–322.

Stout, R.D., Suttles, J., 2004. Functional plasticity of macrophages: reversible adaptation to changing microenvironments. J. Leukoc. Biol. 76 (3), 509–513.

Takeda, M., Kawaguchi, M., Kumatoriya, T., Horiuchi, T., Watanabe, K., Inoue, S., Konishi, N., Furuya, H., 2011. Effects of minocycline on hind-limb motor function and gray and white matter injury after spinal cord ischemia in rats. Spine (Phila Pa 1976) 36 (23), 1919–1924.

Teng, Y.D., Choi, H., Onario, R.C., Zhu, S., Desilets, F.C., Lan, S., Woodard, E.J., Snyder, E.Y., Eichler, M.E., Friedlander, R.M., 2004. Minocycline inhibits contusion-triggered mitochondrial cytochrome c release and mitigates functional deficits after spinal cord injury. Proc. Natl. Acad. Sci. U. S. A. 101 (9), 3071–3076.

Urban, M.W., Ghosh, B., Strojny, L.R., Block, C.G., Blazejewski, S.M., Wright, M.C., Smith, G.M., Lepore, A.C., 2018. Cell-type specific expression of constitutively-active Rheb promotes regeneration of bulbospinal respiratory axons following cervical SCI. Exp. Neurol. 303, 108–119.

Wang, X., Zhu, S., Drozda, M., Zhang, W., Stavrovskaya, I.G., Cattaneo, E., Ferrante, R.J., Kristal, B.S., Friedlander, R.M., 2003. Minocycline inhibits caspase-independent and -dependent mitochondrial cell death pathways in models of Huntington's disease. Proc. Natl. Acad. Sci. U. S. A. 100 (18), 10483–10487.

Wang, X., Cao, K., Sun, X., Chen, Y., Duan, Z., Sun, L., Guo, L., Bai, P., Sun, D., Fan, J., He, X., Young, W., Ren, Y., 2015. Macrophages in spinal cord injury: phenotypic and functional change from exposure to myelin debris. Glia 63 (4), 635–651.

Wang, Z., Nong, J., Shultz, R.B., Zhang, Z., Kim, T., Tom, V.J., Ponnappan, R.K., Zhong, Y., 2017. Local delivery of minocycline from metal ion-assisted self-assembled complexes promotes neuroprotection and functional recovery after spinal cord injury. Biomaterials 112, 62–71.

Wasserman, J.K., Schlichter, L.C., 2007. Minocycline protects the blood-brain barrier and reduces edema following intracerebral hemorrhage in the rat. Exp. Neurol. 207 (2), 227–237.

Wright, M.C., Son, Y.J., 2007. Ciliary neurotrophic factor is not required for terminal sprouting and compensatory reinnervation of neuromuscular synapses: re-evaluation of CNTF null mice. Exp. Neurol. 205 (2), 437–448.

Wright, M.C., Cho, W.J., Son, Y.J., 2007. Distinct patterns of motor nerve terminal sprouting induced by ciliary neurotrophic factor vs. botulinum toxin. J. Comp.

Neurol. 504 (1), 1–16.
Wright, M.C., Potluri, S., Wang, X., Dentcheva, E., Gautam, D., Tessler, A., Wess, J., Rich, M.M., Son, Y.J., 2009. Distinct muscarinic acetylcholine receptor subtypes contribute to stability and growth, but not compensatory plasticity, of neuromuscular synapses. J. Neurosci. 29 (47), 14942–14955.
Wright, M.C., Mi, R., Connor, E., Reed, N., Vyas, A., Alspalter, M., Coppola, G., Geschwind, D.H., Brushart, T.M., Hoke, A., 2014. Novel roles for osteopontin and clusterin in peripheral motor and sensory axon regeneration. J. Neurosci. 34 (5), 1689–1700.
Xue, M., Mikliaeva, E.I., Casha, S., Zygun, D., Demchuk, A., Yong, V.W., 2010. Improving outcomes of neuroprotection by minocycline: guides from cell culture and intracerebral hemorrhage in mice. Am. J. Pathol. 176 (3), 1193–1202.
Zhang, Y.H., Chen, H., Chen, Y., Wang, L., Cai, Y.H., Li, M., Wen, H.Q., Du, J., An, R., Luo, Q.L., Wang, X.L., Lun, Z.R., Xu, Y.H., Shen, J.L., 2014. Activated microglia contribute to neuronal apoptosis in Toxoplasmic encephalitis. Parasit. Vectors 7, 372.
Zhang, Z., Wang, Z., Nong, J., Nix, C.A., Ji, H.F., Zhong, Y., 2015. Metal ion-assisted self-assembly of complexes for controlled and sustained release of minocycline for biomedical applications. Biofabrication 7 (1), 015006.